Photodissociation of CSCl$_2$ at 235 nm: Kinetic energy distributions and branching ratios of Cl atoms and CSCl radicals

Tina S. Einfeld, Christof Maul, and Karl-Heinz Gericke
Institut für Physikalische und Theoretische Chemie, Technische Universität Braunschweig, Hans-Sommer-Straße 10, D-38106 Braunschweig, Germany

Alexei Chichinin
Institut für Physikalische und Theoretische Chemie, Technische Universität Braunschweig, Hans-Sommer-Straße 10, D-38106 Braunschweig, Germany and Institute of Chemical Kinetics and Combustion, 630090 Novosibirsk, Russia

The photodissociation dynamics of thiophosgene (CSCl$_2$) and the respective branching ratios of both dissociation products Cl and CSCl have been studied by 3D imaging of the photodissociation product chlorine in its ground state $^2P_{3/2}$[Cl] and excited spin–orbit state $^2P_{1/2}$[Cl*] employing the resonance enhanced multiphoton ionization and time-of-flight technique at a dissociation wavelength of about 235 nm. A novel technique is applied where the complete three-dimensional (3D) momentum vector of a reaction product is directly determined. The kinetic energy distribution (KED) for Cl* is observed for the first time. The obtained KEDs of Cl and Cl* are different in the low kinetic energy range due to the correlating state of the partner fragment CSCl. In the case of ground state Cl the CSCl partner radical is produced in the ground $\widetilde{X}$, $\widetilde{A}$, and $\widetilde{B}$ states with a contribution of 4±0.5%, 60±5%, and 36±3%, respectively. In the case of Cl* the corresponding CSCl is produced with a contribution of 7.5±0.5% in the ground $\widetilde{X}$, 71.5±5.5% in state $\widetilde{A}$, and 21±1.5% in state $\widetilde{B}$. The yield of Cl*, $\phi(\text{Cl*}) = P(\text{Cl*})/[P(\text{Cl}) + P(\text{Cl*})]$, was found to be 0.47. No significant velocity dependence of the anisotropy parameter β could be observed. The mean value +0.03 suggests a decay on the $\widetilde{B}$ (A_1) surface. © *2002 American Institute of Physics.*
[DOI: 10.1063/1.1480272]

I. INTRODUCTION

The implication of a novel 3D imaging technique that allows us to monitor the full three-dimensional momentum vectors of individual products of a chemical elementary reaction[1] has led to a detailed examination of the ultraviolet photodissociation of a series of tetra-atomic starlike molecules[2–4] which can, in principle, decay into three fragments. Adequate projection methods allow us to extract state-specific fragment kinetic energy distributions as well as the anisotropy parameter β describing the spatial fragment distribution from the 3D momentum data. The determination of the velocity dependence of the anisotropy parameter proved to be especially useful in the analysis of competing two- and three-body channels in the photodissociation of SOCl$_2$ (Refs. 3 and 4) and COCl$_2$.[2,5] We present here a study of the structurally similar thiophosgene (CSCl$_2$) molecule which offers the possibility to investigate a different electronic transition than in the phosgene case at the same dissociation energy.

Thiophosgene, CSCl$_2$, has been the object of extensive studies both in the gas phase and in solution because it offers insight into several important aspects of electronic spectroscopy, photophysics, and photochemistry.[6–16] One advantage of thiophosgene is its thermal stability and ready availability. The structure of its ground state ($\widetilde{X}$ $^1A_1$) in C_{2v} symmetry is well known.[17] The electron configuration of the general state has been determined by photoelectron spectroscopy to be

[core] $(9a_1)^2(10a_1)^2(6b_2)^2(11a_1)^2(7b_2)^2(3b_1)^2(12a_1)^2$ $\times(2a_2)^2(8b_2)^2(13a_1)^2(4b_1)^2(9b_2)^2$, where the $9a_1$, $6b_2$, and $10a_1$ molecular orbitals (MOs) contain the σ bonding electrons, the $3b_1$ and the $4b_1$ orbitals are a combination of the π bonding electrons and Cl($3p$) electrons, and the $9b_2$ and $13a_1$ MOs contain the sulfur lone pair electrons.[18] The thiophosgene absorption spectrum as shown in Fig. 1 was reported by Farnworth and King.[19] Thiophosgene absorbs weakly in the visible region to produce the lowest triplet and lowest excited singlet states, T_1 ($\widetilde{a}$ $^3A_2$) and S_1 ($\widetilde{A}$ $^1A_2$), respectively, which corresponds to a symmetry-forbidden $\pi^*_{CS} \leftarrow n_S(5b_1 \leftarrow 9b_2)$ electron promotion. Illumination in the strong band system in the near-UV region populates the second excited singlet state, S_2 ($\widetilde{B}$ $^1A_1$), which arrives from the allowed promotion of a $4b_1$ electron to the $5b_1$ MO. The $\widetilde{B}(^1A_1) \leftarrow \widetilde{X}(^1A_1)$ transition is therefore partially $\pi^*_{CS} \leftarrow \pi_{CS}$ in character, and results in lowering the C–S bond order, lengthening the equilibrium C–S bond length by about 0.5 Å, and decreasing of the Cl–Cl bond angle from 111.2° to 103°.[20] The Farnworth and King[19] analysis indicated that the molecule is nonplanar in the upper $^1A_1$ state with an out-of-plane angle of 20° and an inversion barrier of 126 cm^{-1}. Studies of the gas-phase photochemistry[14,15] and photophysics[21] of thiophosgene have flourished since the discoveries of fluorescence from both the S_1 ($\widetilde{A}$ $^1A_2$) and S_2 ($\widetilde{B}$ $^1A_1$) states.[22,23] The fluorescence from the first singlet S_1 and the second singlet S_2 has been observed at wavelength
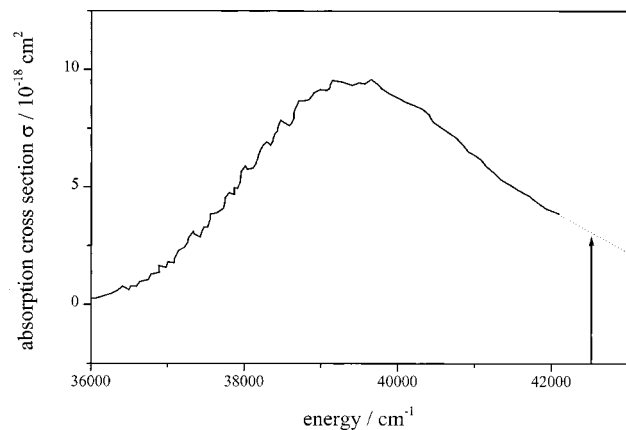
        1123

FIG. 1. Absorption cross section of $CSCl_2$ (Ref. 19), the photon energy used in the present experiment is marked by an arrow. Due to the lack of experimental data, the absorption cross section in the high energy range is extrapolated and presented by a dotted curve.

above 455 nm (Refs. 23 and 24) and 277 nm (Refs. 22 and 23), respectively. The spectrum in the 240–287.5 nm region shows no fine structure and only the vibrational spectrum is apparent down to 268 nm.[19] Below this wavelength the bands become very diffuse, indicating increasing predissociation of the upper state within 10^{-13} s.[14]

Excitation at higher energies (e.g., $\lambda = 248$ nm) does not produce observable fluorescence, but results exclusively in photodissociation. The mechanism of the photodissociation of this tetra-atomic molecule can be characterized by three possible decay mechanisms. For the photodissociation of $CSCl_2$ above 200 nm, the radical (1.1) and molecular channel (1.2) produces two fragments,

$$CSCl_2 + h\nu \rightarrow Cl(^2P_J) + CSCl(\widetilde{X}, \widetilde{A}, \widetilde{B}), \qquad (1.1)$$

$$CSCl_2 + h\nu \rightarrow Cl_2(^1\Sigma_g^+) + CS(^1\Sigma), \qquad (1.2)$$

Below 221 nm the excitation energy exceeds the energy required to break both Cl–C bonds, and three-body dissociation[25] (1.3) may also take place,

$$CSCl_2 + h\nu \rightarrow 2Cl(^2P_J) + CS(^1\Sigma). \qquad (1.3)$$

Other than in phosgene, excitation at 235 nm will not access the lowest $^1A_2$ state, but the second absorption band associated with the $^1A_1$ state. The absorption cross section is much stronger $[\sigma_{235}(CSCl_2) = 4 \times 10^{-18}$ cm^{-1}, $\sigma_{235}(COCl_2) = 9 \times 10^{-20}$ cm$^{-1}]$ because contrary to $COCl_2$ the $CSCl_2$ transition is symmetry-allowed. The wavelength shift in the absorption spectrum is due to the substitution of the oxygen atom by a sulfur atom. The relative weakness of the C–S bond goes along with a strengthening of the C–Cl bond, and the three-body threshold is increased such that the three-body channel (1.3) is not accessible at a dissociation wavelength of 235 nm. Thus, a similar situation is created as in the photodissociation of COFCl, where the substitution of a chlorine by a fluorine atom also closes the three-body decay channel.[26] Contrarily to the case encountered here, the accessed state for COFCl was the same $^1A_2$ state as in phosgene so that by chemical substitution the first step of a three-body break-up could individually be studied.

CSCl and Cl_2 fragments were detected from 248 nm laser photolysis of a pulsed molecular beam of $CSCl_2$.[15] These fragments formed under collision free conditions were explained by two decomposition pathways: reactions (1.1) and (1.2). The quantum yield for (1.1) was found to be 0.8 ± 0.1 and the experimental energy release E_T / E_{av} 0.29 ± 0.02, where E_T is the averaged total translational energy and E_{av} the maximal energy available to the fragments after dissociation. The observed translational energy release was only in modest agreement with the calculation of 0.37 which was predicted by employing the impulsive spectator model.[27] This deviation led Hachey *et al.*[16] to question, whether the original assumption was correct that only ground-state, bent CSCl radicals could be produced in reaction (1.1). Calculations by Chan and Goddard[28] and by Hachey *et al.*[16] showed that a very low lying excited singlet linear state is thermodynamically accessible. Hachey *et al.* re-evaluated via *ab initio* CI studies the geometry of the ground and the first electronically excited states of the CSCl radical, the vertical excitation energies of its ten lowest doublet states and two lowest quartet states to construct a more complete energy level correlation diagram. These studies show that the three possible states $\widetilde{X}$, $\widetilde{A}$, and $\widetilde{B}$ of the CSCl fragment can be assessed in the UV photofragmentation of $CSCl_2$ which are already introduced in the reaction scheme of the radical delay channel (1.1).

Despite this, the question about their relative importance has not yet been answered. In the present work the photofragmentation dynamics of $CSCl_2$ are studied when irradiated around 235 nm. The purpose of the present work is to determine (i) the complete 3D velocity distribution for both ground state Cl and excited state Cl* and the respective anisotropy parameter β, (ii) the contribution of the $\widetilde{X}$, $\widetilde{A}$, and $\widetilde{B}$ states of CSCl, and (iii) the spin–orbit branching ratio of Cl*/Cl.

II. EXPERIMENT

A more detailed description of the experimental setup and the novel position sensitive detector (PSD) has been published elsewhere.[1,2] Briefly it consists of a combination of a homebuilt single-field time-of-flight (TOF) mass-spectrometer and a position sensitive detector.[29–31] The spectrometer was evacuated to a base pressure of $\sim 10^{-8}$ mbar by a turbomolecular pump system. Thiophosgene was constantly cooled to $\sim 20\,°C$ to prepare a mixture of about 0.5% $CSCl_2$ in helium. The mixture was fed into the spectrometer via a continuous supersonic beam as well as under bulk conditions, yielding the same results. With a nozzle diameter of 20 μm and a stagnation pressure of ~ 3 bar typical working pressures were in the order of 10^{-7} mbar. Under these conditions the beam is characterized by a rotational temperature of about 8 K, determined by a rotationally resolved calibration spectrum of the NO ($A\ ^2\Sigma^+ \leftarrow X\ ^2\Pi$) transition.[1]

Simultaneous dissociation and state-selective detection of chlorine atoms were performed using one dye laser pumped by a Nd:YAG laser (Coherent, Infinity 40 100). The dye laser (Lamba Physik, Scanmate) was operated with Coumarin 47 at a repetition rate of 100 Hz, its light was frequency-doubled by a BBO crystal and focused by a 20 cm

lens in order to decrease the reaction volume to 5×10^{-4} mm^3. The energy of the frequency-doubled light amounted to 5–10 μJ per pulse. The energy was kept low to obtain approximately one fragment signal per ten laser pulses to avoid kinetic energy transfer to the fragments due to space charge effects and saturation of the dissociation step. The laser beam, the molecular beam, and the detector axes were mutually orthogonal in the interaction region. Ultimate care was taken to overlap the light and the molecular beam which was checked frequently by monitoring of NO via (1+1) resonance enhanced multiphoton ionization (REMPI) at 226 nm and optimizing of the signal intensity.[32] The polarization of the laser was changed by a half-wave plate in order to investigate the spatial fragment distribution. Typically the acceleration voltage was 800 V in the acceleration tube of the TOF spectrometer corresponding to an acceleration field of 16 kV/m.
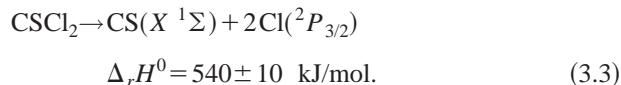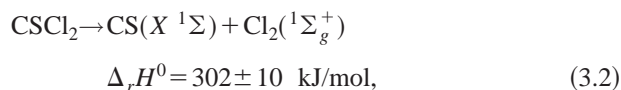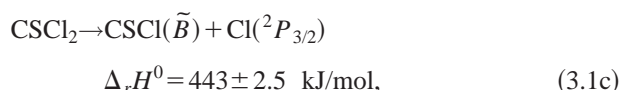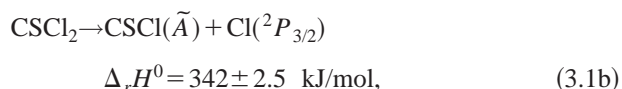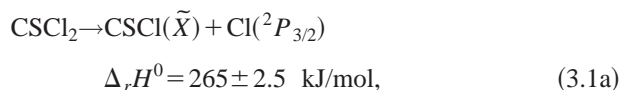
The ^2P_J state of the chlorine atom is split by 882 cm^{-1} due to spin–orbit coupling into Cl($^2P_{3/2}$) and Cl*($^2P_{1/2}$). Both states were detected by a (2+1) REMPI process. The ground state was probed via the ($^2D_{3/2} \leftarrow {}^2P_{3/2}$) transition at 235.336 nm, the excited state by the ($^2P_{1/2} \leftarrow {}^2P_{1/2}$) transition at 235.205 nm. Typically the dye laser was scanned over a range of ± 0.003 nm around the center transitions accounting for the Doppler broadening. Signals were digitized by time-to-digital converters (TDCs), accumulated over 2×10^5 laser shots, and saved on-line by a personal computer. The analyzing procedure is described in detail elsewhere.[2]

The PSD includes a delay-line anode (DLA) introduced into the spectrometer chamber right behind the double stage microchannel plates (MCPs). The PSD allows us to monitor all three components of the momentum vector from the measured position of one particle on the detector and its corresponding time-of-flight (TOF). Therefore, a full 3D velocity distribution is observed and the complete information about the kinetic energy distribution and the velocity dependent anisotropy parameter β can be extracted.

III. RESULTS AND DISCUSSION

The $\widetilde{B}(^1A_1) - \widetilde{X}(^1A_1)$ band system of CSCl$_2$ molecules has been extensively studied by spectroscopists[8,9,16,33] who found that the onset of predissociation required 427.4 ± 0.6 kJ/mol, i.e., 17.3 ± 0.6 kJ/mol above the $\widetilde{B}(^1A_1)$ state.

Reaction enthalpies $\Delta_r H$ for the three photodissociation channels of CSCl$_2$ are calculated from the enthalpies of formation $\Delta_f H$ of the reactants,

$$CSCl_2 \rightarrow CSCl(\widetilde{X}) + Cl(^2P_{3/2})$$

$$\Delta_r H^0 = 265 \pm 2.5 \text{ kJ/mol}, \tag{3.1a}$$

$$CSCl_2 \rightarrow CSCl(\widetilde{A}) + Cl(^2P_{3/2})$$

$$\Delta_r H^0 = 342 \pm 2.5 \text{ kJ/mol}, \tag{3.1b}$$

$$CSCl_2 \rightarrow CSCl(\widetilde{B}) + Cl(^2P_{3/2})$$

$$\Delta_r H^0 = 443 \pm 2.5 \text{ kJ/mol}, \tag{3.1c}$$

$$CSCl_2 \rightarrow CS(X\ ^1\Sigma) + Cl_2(^1\Sigma_g^+)$$

$$\Delta_r H^0 = 302 \pm 10 \text{ kJ/mol}, \tag{3.2}$$

$$CSCl_2 \rightarrow CS(X\ ^1\Sigma) + 2Cl(^2P_{3/2})$$

$$\Delta_r H^0 = 540 \pm 10 \text{ kJ/mol}. \tag{3.3}$$

There are some uncertainties in the enthalpies of formation $\Delta_f H^0$ for the CSCl$_2$ and CSCl molecules. For this study, the $\Delta_f H^0$ of the CS radical was adopted from the most recent literature source.[34] The $\Delta_f H^0$ of CSCl$_2$ and CSCl ($\widetilde{X}$, $\widetilde{A}$, and $\widetilde{B}$) were obtained from Joshi[35] and Hachey et al.,[16] respectively. Hachey et al. based the calculation of $\Delta_f H^0$ of the different CSCl states on the publication of Okabe,[14] who determined the bond energy D_0 (SClC–Cl) to be 265 ± 2.5 kJ/mol. The enthalpies $\Delta_r H^0$ of the reactions above were calculated for the spin–orbit ground state Cl, so $\Delta_r H^0$ required for the generation of one Cl* atom is higher by 10.6 kJ/mol.

As the molecular channel (3.2) cannot be observed in our experiment and the three-body decay channel (3.3) is energetically not allowed at the wavelength of 235 nm, we concentrated on the three details of the two-body decay channel (3.1), the spin–orbit branching ratio of Cl*/Cl, and the relative importance of the different states of CSCl which are not yet established with certainty.[36]

A. Spin–orbit branching ratio Cl*/Cl

The spin–orbit branching ratio was obtained by scanning the laser over the two resonance transitions of Cl and Cl*. The measurements were repeated at different laser light intensities. Integrating the area under the Doppler profiles results in a signal ratio $S(\text{Cl*})/S(\text{Cl})$ of 0.80 ± 0.04. Taking the ratio of transition probabilities B of 1.06 (Ref. 37) into account we determined a Cl* yield $\phi(\text{Cl*}) = 0.47 \pm 0.03$, where ϕ is defined as the ratio of the number of excited state atoms $P(\text{Cl*})$ to the total number of chlorine atoms, $\phi(\text{Cl*}) = P(\text{Cl*})/[P(\text{Cl}) + P(\text{Cl*})]$. On statistical grounds one expects a yield of $\phi_{\text{statistical}} = 0.33$.

B. Fragment kinetic energy and angular distribution

In Fig. 2 the kinetic energy distributions (KEDs) and the anisotropy parameter β are presented for the photodissociation of thiophosgene around 235 nm for both spin–orbit states. Here β, the anisotropy parameter ranging from -1 (perpendicular transition) to $+2$ (parallel transition), characterizes the spatial fragment distribution $P(\theta, v) \propto f(v)(1 + \beta(v)P_2(\cos\theta))$, where θ is the angle of the polarization vector of the dissociating laser with the product recoil velocity vector, and P_2 is the second Legendre polynomial, $P_2(x) = \frac{1}{2}(3x^2 - 1)$. The 1D KED presentation is obtained via integration of the 3D data, while for the anisotropy parameter β the velocity dependency is evaluated from the 3D data subdivided into velocity ranges of 200 m/s. Although both Cl and Cl* are released with kinetic energies in the whole available energy range up to the calculated limit of 170 kJ/mol, a remarkably different behavior of the two spin components with respect to their kinetic energy acquisition in the photodissociation is obvious. The KED of ground state
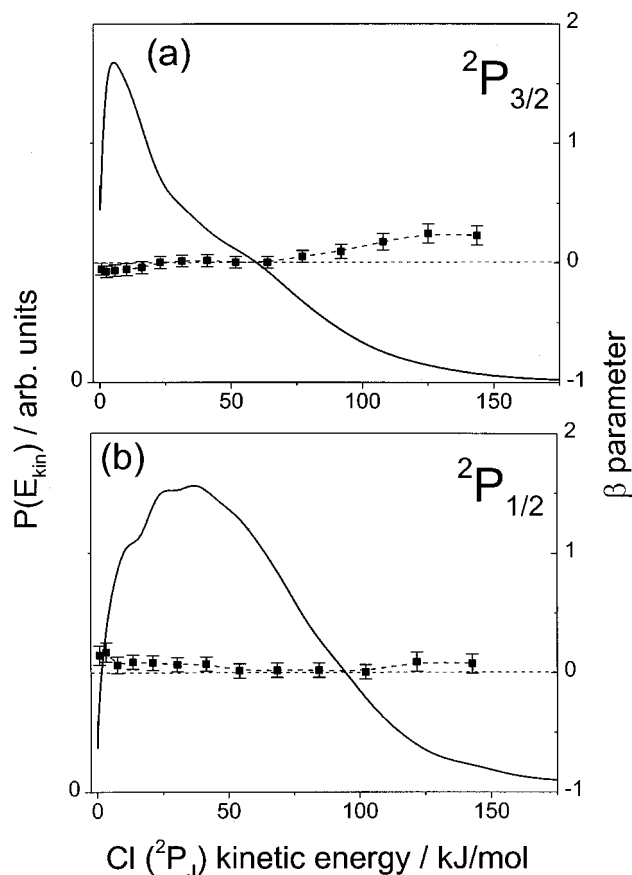
FIG. 2. Kinetic energy distribution for (a) ground state Cl($^2P_{3/2}$) and (b) excited state Cl*($^2P_{1/2}$) atoms produced in the photodissociation of CSCl$_2$ at 235 nm. The dependence of the β parameter on the Cl fragment kinetic energy (right scale) is shown by curves with error bars. This 1D presentation is obtained via integration of the 3D data.

Cl is bimodal releasing Cl mainly with low kinetic energy, where a shoulder is obtained at intermediate energy range with a tail reaching the high energy range. In comparison the KED of excited state Cl* is broad showing no preference for very low kinetic energies. No fine structure is observed over the whole energy range. The maximal available kinetic energy of one Cl fragment is calculated from the bond energy of 265.3 kJ/mol given by Okabe[14] assuming that the partner fragment SCCl has no internal energy.

Chlorine is almost isotropically released: The spatial fragment distribution is characterized by very small averaged β parameters of 0.01 ± 0.05 and 0.06 ± 0.06 for Cl and Cl*,

respectively. The β parameters are almost velocity independent within the experimental error, only a very small increase is observed at very high kinetic energies (see Fig. 2 and Table I). The theoretical limit for the β parameter for an instantaneous decay from the excited $^1A_1$ state geometry with a Cl–C–Cl bond angle of 103° (Ref. 20) is 0.08. The respective transition dipole moment μ is oriented along the C_2 axis containing the CS bond. Although lack of anisotropy can be due to an excited state lifetime longer than a rotational period, the geometry of the molecule and the transition moment resulting in a half bond angle between Cl–Cl close to the magic angle $\theta_m = 54.7°$ with $P_2(\cos \theta_m) = 0$, could cause an isotropic fragment distribution, even if the dissociation is direct. In agreement with Ondrey and Bershohn[15] it is concluded that the dissociation proceeds directly and fast via the excited $^1A_1$ state of ground state geometry.

C. CSCl energy disposal

The internal energy of CSCl is not measured directly. However, via the relation,

$$E_{int}(CSCl) = E_{av} - E_T - E_{int}(Cl), \tag{3.4}$$

$E_{int}(CSCl)$ can be determined by transforming the measured KED of both Cl and Cl* into the internal energy distribution (IED) of the respective partner fragments CSCl by conservation of linear momentum and energy according to

$$E_T = \left(1 + \frac{m_{Cl}}{m_{CSCl}}\right) E_{kin}(Cl). \tag{3.5}$$

The available energies E_{av} in Eq. (3.4) is given by the photolysis energy $h\nu$ and the dissociation energy $D_0(SClC–Cl)$. The internal energy of the parent molecule $E_{int}(CSCl_2)$ is negligible,

$$E_{av} = h\nu - D_0(SClC–Cl). \tag{3.6}$$

The obtained IEDs via Eq. (3.4) are shown in Fig. 3 and characteristic data are summarized in Table I. Three Gaussians are fitted to these internal energy distributions with respect to the calculations of the $\tilde{X}$, $\tilde{A}$, and $\tilde{B}$ state of Hachey *et al.*[16] Based on the Gaussians fit, the internal energies of the three electronical states can be calculated. Two aspects must be taken into account: First, the low internal energy flanks of the Gaussians reaching the energetic forbidden region must be excluded. The energetic limits are marked in Fig. 3 by a dotted line for the $\tilde{A}$ and by a dashed line for the

TABLE I. Characteristic data describing the kinetic energy distribution of Cl and Cl*, and the internal energy distribution of the partner fragment CSCl, the β parameter, the branching ratios of the CSCl fragment and the kinetic energy release $E_T/(E_{av}-E_{el})$ in the photodissociation of CSCl$_2$. $E_{av}(Cl+CSCl) = 243$ kJ/mol, $E_{av}(Cl*+CSCl) = 232.4$ kJ/mol, $E_{el}(\tilde{A}) = 77$ kJ/mol, $E_{el}(\tilde{B}) = 178$ kJ/mol.

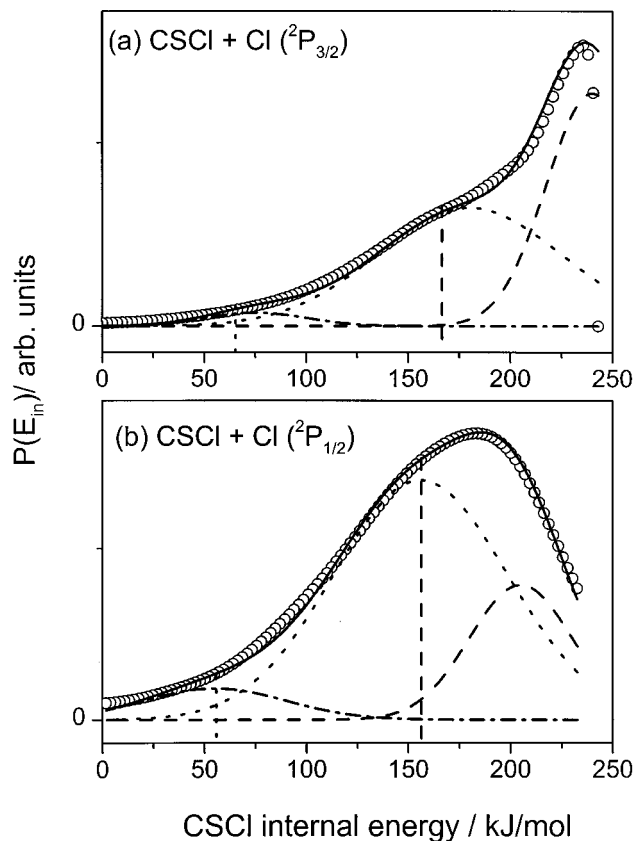| Fragment	Correlating CSCl states	Contribution (%)	E_{int} (kJ/mol)	E_T (kJ/mol)	$E_T/(E_{av}-E_{el})$	β parameter
Cl	($\tilde{X}$)	2	75	168	0.69 ± 0.04	0.2 ± 0.07
	($\tilde{A}$)	32	98	68	0.41 ± 0.03	0.03 ± 0.05
	($\tilde{B}$)	19	47	18	0.28 ± 0.03	-0.07 ± 0.06
Cl*	($\tilde{X}$)	3.5	57	175	0.75 ± 0.05	0.08 ± 0.07
	($\tilde{A}$)	33.5	77	78	0.50 ± 0.03	0.03 ± 0.06
	($\tilde{B}$)	10	23	31	0.57 ± 0.04	0.15 ± 0.08

FIG. 3. Internal energy distribution of CSCl for both Cl (a) and Cl* (b) partner fragments. The energetic limits taken from Ref. 17 are marked by a dotted and a dashed line for the $\tilde{A}$ and $\tilde{B}$ state of CSCl, respectively. Remarkable is the different curve shape especially in the high internal energy region. Three Gaussians are fitted to the distribution in order to evaluate the contributions of the different electronic states of CSCl. The dashed line is assigned to the $\tilde{B}$ state, the dotted line to the $\tilde{A}$ state, and the dot-dashed line to the $\tilde{X}$ state.
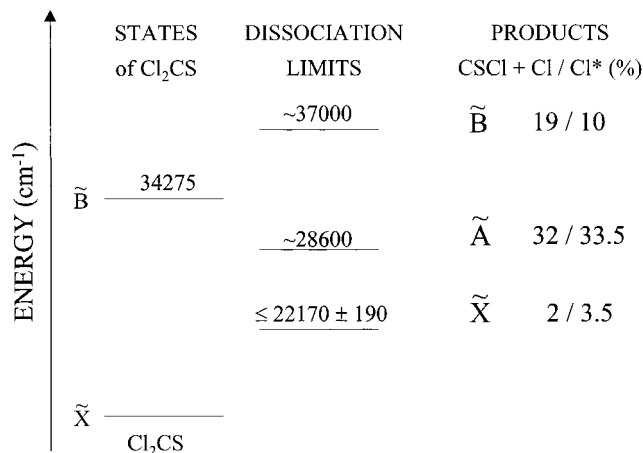

FIG. 4. Energy level diagram for CSCl₂ and its dissociation products taken from Hachey *et al.* (Ref. 17). The energy levels are given relative to the ground state $\tilde{X}$ of CSCl₂. The observed correlation to the ground or excited state of chlorine in the products are added.

$\tilde{B}$ state of CSCl. This energetic restriction has only a minor effect on the calculated internal energies of CSCl($\tilde{X}$), CSCl($\tilde{A}$), and CSCl($\tilde{B}$). Second, the maximal energy of 243 kJ/mol limits the Gaussians at high energies. This influences essentially the contribution of CSCl($\tilde{B}$). The total internal E_{int} (including the electronic energy of the $\tilde{A}$ and $\tilde{B}$ state) is accordingly calculated to be 225, 175, and 75 kJ/mol, which are assigned to CSCl($\tilde{B}$)+Cl, CSCl($\tilde{A}$)+Cl, and CSCl($\tilde{X}$)+Cl, respectively, and 201, 154, and 57 for CSCl($\tilde{B}$)+Cl*, CSCl($\tilde{A}$)+Cl*, and CSCl($\tilde{A}$)+Cl*. Considering the electronic energy E_{el} of 77 kJ/mol for the $\tilde{A}$ state and 178 kJ/mol for the $\tilde{B}$ state of the CSCl, one obtains for the Cl($^2P_{3/2}$) channel an internal energy release of 75 kJ/mol for CSCl($\tilde{X}$), 98 kJ/mol for CSCl($\tilde{A}$), and 47 kJ/mol for CSCl($\tilde{B}$). For the Cl* channel one obtains the respective values of 57, 77, and 23 kJ/mol.

In addition, the state specific kinetic energy release $\langle E_T \rangle / (E_{av} - E_{el})$ can be calculated. Since the state specific E_T is obtained via E_{int} resulting in $E_T = 168$, 69, and 18 kJ/mol for reaction (1a), (1b), and (1c), respectively, releasing ground state Cl, the total kinetic energy release $\langle E_T \rangle / (E_{av} - E_{el})$ is evaluated to be 0.69 ± 0.04, 0.42 ± 0.03,

and 0.28 ± 0.02 for CSCl($\tilde{X}$)+Cl, CSCl($\tilde{A}$)+Cl, and CSCl($\tilde{B}$)+Cl, respectively. In the case of excited state Cl* the energy release $\langle E_T \rangle / (E_{av} - E_{el})$ is 0.75 ± 0.05, 0.51 ± 0.03, and 0.59 ± 0.03, where E_T is 175, 79, and 32 kJ/mol for CSCl($\tilde{X}$)+Cl*, CSCl($\tilde{A}$)+Cl*, and CSCl($\tilde{B}$)+Cl*. The obtained energy releases are summarized in Table I.

It is concluded that the simple impulsive spectator model[38] predicting a value of $\langle E_T \rangle / E_{av} = 0.369$ cannot be used for describing the photodissociation of CSCl₂ at ~235 nm in detail. This conclusion is supported by the geometry change upon exciting CSCl₂ from its ground state $\tilde{X}(^1A_1)$ to its excited state $\tilde{B}(^1A_1)$ being evidence of a strong gradient of the upper potential energy surface with respect to the angle γ describing the out-of-plane bending of CSCl₂ compared to the planar ground state geometry.[39]

D. Spin correlation of the CSCl partner fragment

The obtained internal energy distributions for the partner fragment CSCl of the ground and excited state Cl atoms, shown in Fig. 3, allow us to study the contribution of the involved states CSCl($\tilde{X}$), CSCl($\tilde{A}$), and CSCl($\tilde{B}$), calculated by Chan and Goddard[28] and Hachey *et al.*[6,16] Figure 4 shows the energy values[16] for our present study.

The overall contributions of the CSCl $\tilde{X}$, $\tilde{A}$, and $\tilde{B}$ states can be determined by the three Gaussians which are fitted to the IED taking the calculation by Hachey into account. Integrating the area under the Gaussian profiles yield the ratio of 1:13:6 for CSCl($\tilde{X}$):CSCl($\tilde{A}$):CSCl($\tilde{B}$), summed over both chlorine atom spin–orbit states. Clearly, the generation of CSCl($\tilde{X}$) is only a minor channel. In the case of ground state Cl, the states $\tilde{X}$, $\tilde{A}$, and $\tilde{B}$ of CSCl contribute to 1:15:9, respectively. Cl in its ground state is predominantly released with a CSCl partner fragment with high internal energy up to the energetic limit. In the case of spin–orbit excited Cl* the contributions of the states $\tilde{X}$, $\tilde{A}$, and $\tilde{B}$ of CSCl are 1:9.5:2.8, respectively.

The observed contribution of the different CSCl states allows to speculate that $CSCl_2$ would decay into three fragments releasing two slow ground state Cl, if the three-body threshold will be passed by increasing the photolysis energy. With respect to Cl* the shape of the contribution (lower panel of Fig. 3) suggests that Cl* would be released as a minor product if the three-body decay channel is energetically allowed. This view is further supported by the CSCl state-specific $P(Cl^*)/P(Cl)$ branching ratios which drop from 1.6 for the $\widetilde{X}$ to 1.2 for the $\widetilde{A}$ state, and to 0.6 for the $\widetilde{B}$ state.

In addition, due to the geometry change upon exciting $CSCl_2$ a significant rotational excitation of the electronically excited CSCl radical seems likely, with a tendency to realize a three-body decay as soon as the respective threshold energy is surpassed. A large internal fragment excitation favoring a three-body decay upon transgressing the three-body threshold was observed for $COCl_2$ and COFCl upon excitation in the first absorption bands associated with the $^1A_2$ state. The same behavior is also found upon excitation of the $^1A_1$ band of $CSCl_2$. Whereas different electronic excitations are involved they have the same excited π^*_{CS} molecular orbital in common. The observations on $CSCl_2$ in conjunction with the observations on $COCl_2$ and COFCl therefore suggest that the tendency towards exhibiting an early three-body decay is linked to the excitation of a π^* electron in the double bond on the far side of the molecule, i.e., opposite to the bonds that are to be broken. A subsequent rearrangement of the energy initially deposited in the CS bond channels a significant portion into the dissociation coordinate of the intermediate CSCl fragment leading to its eventual unimolecular decay. In agreement with the above, in the vibrationally mediated dissociation of $CHFCl_2$ (Ref. 40) and CH_3CFCl_2 (Ref. 41) vibrational energy initially deposited in the CH vibrational degrees of freedom is redistributed to all degrees of freedom of the intermediate after departure of the first Cl fragment. Due to the large number of degrees of freedom not associated with the dissociation coordinate, the contribution of three-body decay was small for $CHFCl_2$ and almost absent for CH_3CFCl_2. This supports our view that the excitation of the far double bond tends to produce a sequential or at least a slow concerted three-body decay in small polyatomic molecules such as carbonyl halides and related species.

IV. CONCLUSION

The photodissociation of $CSCl_2$ at 235 nm was studied by a novel REMPI-TOF-3D imaging technique. The 3D velocity distribution of excited state Cl* and ground state Cl and the respective anisotropy parameters β as a function of the recoil velocity were measured. The β parameter was found to be essentially velocity independent with an averaged value of 0.03 ± 0.06.

The kinetic energy distribution of the ground state Cl is bimodal releasing Cl mainly with low kinetic energy, whereas the KED of the excited state Cl* is broad showing no preference for very low kinetic energies.

The kinetic energy distributions of Cl and Cl* include the information of the corresponding states of the CSCl part-

ner fragment. It was found that the main partner of both Cl and Cl* is CSCl in the excited state $\widetilde{A}$ and $\widetilde{B}$, and the generation of $CSCl(\widetilde{X})$ is only a minor channel. Considering the electronic energy E_{el} of 77 kJ/mol for the $\widetilde{A}$ state and 178 kJ/mol for the $\widetilde{B}$ state of the CSCl, an internal energy release of 75 kJ/mol for $CSCl(\widetilde{X})$, 98 kJ/mol for $CSCl(\widetilde{A})$, and 47 kJ/mol for $CSCl(\widetilde{B})$ is evaluated if the Cl partner is generated in its ground state. For the Cl* channel respective values of 57, 77, and 23 kJ/mol are obtained. By taking the spin–orbit branching ratio of $P(Cl^*)/[P(Cl)+P(Cl^*)]$ of 0.47 into account, the absolute values of the contribution of $\widetilde{X}$, $\widetilde{A}$, and $\widetilde{B}$ states are $5.5\pm0.5\%$, $65.5\pm5\%$, and $29\pm3\%$, respectively.

The energy release $E_T/(E_{av}-E_{el})$ was found to be 0.69 ± 0.04, 0.42 ± 0.03, and 0.28 ± 0.02 for ground state Cl and $CSCl(\widetilde{X})$, $CSCl(\widetilde{A})$, and $CSCl(\widetilde{B})$, respectively, and 0.75 ± 0.05, 0.51 ± 0.03, and 0.59 ± 0.03 for spin excited Cl* and $CSCl(\widetilde{X})$, $CSCl(\widetilde{A})$, and $CSCl(\widetilde{B})$. A significant rotational excitation of the electronically excited CSCl radical seems likely followed by a three-body decay as soon as the respective threshold is surpassed.

[1] A. Chichinin, T. Einfeld, C. Maul, and K.-H. Gericke, Rev. Sci. Instrum. **73**, 1856 (2002).
[2] T. Einfeld, A. Chichinin, C. Maul, and K.-H. Gericke, J. Chem. Phys. **116**, 2803 (2002).
[3] T. Einfeld, A. Chichinin, C. Maul, and K.-H. Gericke (in preparation).
[4] M. Kawasaki, K. Kasatani, H. Sato, H. Shinohara, N. Nishi, H. Ohtoshi, and I. Tanaka, Chem. Phys. **91**, 285 (1984); G. Baum, C. S. Effenhauser, P. Felder, and J. R. Huber, J. Phys. Chem. **96**, 756 (1992); M. Kawasaki, K. Suto, Y. Sato, Y. Matsumi, and R. Bersohn, *ibid.* **100**, 19 853 (1996); C. Maul and K.-H. Gericke, J. Phys. Chem. A **104**, 2531 (2000).
[5] C. Maul, T. Haas, and K.-H. Gericke, J. Chem. Phys. **102**, 3238 (1995); C. Maul, T. Haas, and K.-H. Gericke, J. Phys. Chem. A **101**, 6619 (1997).
[6] A. Maciejewski and R. P. Steer, Chem. Rev. **93**, 67 (1993).
[7] D. J. Clouthier and D. C. Moule, Top. Curr. Chem. **150**, 167 (1989).
[8] B. Simard, V. J. MacKewnzie, P. A. Hackett, and R. P. Steer, Can. J. Chem. **72**, 745 (1994).
[9] M. Ludwiczak, D. R. Latimer, and R. P. Steer, J. Mol. Spectrosc. **147**, 414 (1991).
[10] A. Maciejewski, M. Szymanski, and R. P. Steer, Chem. Phys. **165**, 101 (1992).
[11] K. J. Falk, S. E. Sveinson, and R. P. Steer, Chem. Phys. Lett. **163**, 490 (1989).
[12] M. Szymanski, S. E. Sveinson, and R. P. Steer, J. Phys. Chem. **95**, 5159 (1991).
[13] A. Maciejewski, M. Szymanski, and R. P. Steer, J. Chem. Soc., Faraday Trans. **89**, 3251 (1993).
[14] H. Okabe, J. Chem. Phys. **79**, 175 (1983).
[15] G. S. Ondrey and R. Bersohn, J. Chem. Phys. **79**, 175 (1983).
[16] A. Hachey, F. Grein, and R. P. Steer, Can. J. Chem. **71**, 112 (1993).
[17] J. H. Carpenter, D. F. Rimmer, J. G. Smith, and D. H. Whiffen, J. Chem. Soc., Faraday Trans. 2 **71**, 1752 (1975).
[18] D. Chadwick, Can. J. Chem. **50**, 737 (1972).
[19] E. R. Farnworth and G. W. King, J. Mol. Spectrosc. **57**, 215 (1975).
[20] R. Bigwood, B. Milam, and M. Gruebele, Chem. Phys. Lett. **287**, 333 (1998).
[21] D. C. Moule and C. R. Subramaniam, J. Mol. Spectrosc. **48**, 336 (1973).

[22] T. Oka, A. R. Knight, and R. P. Steer, J. Chem. Phys. **63**, 2414 (1975); D. J. Clouthier, P. A. Hackett, A. R. Knight, and R. P. Steer, J. Photochem. **17**, 319 (1981); D. J. Clouthier, A. R. Knight, R. P. Steer, and P. A. Hackett, J. Chem. Phys. **72**, 1560 (1980); D. M. Brenner, M. N. Spencer, and J. I. Steinfeld, *ibid.* **78**, 136 (1983).

[23] J. R. McDonalds and L. E. Brus, Chem. Phys. Lett. **16**, 587 (1972); S. Z. Levine, A. R. Knight, and R. P. Steer, *ibid.* **29**, 73 (1974).

[24] J. C. D. Brand, J. L. Hardwick, and K. E. Teo, J. Mol. Spectrosc. **57**, 215 (1975).

[25] C. Maul and K.-H. Gericke, Int. J. Radiat. Phys. Chem. **16**, 1 (1997).

[26] C. Maul, C. Dietrich, T. Haas, and K.-H. Gericke, Phys. Chem. Chem. Phys. **1**, 1441 (1999).

[27] G. E. Busch and K. R. Wilson, J. Chem. Phys. **56**, 3638 (1972).

[28] W. T. Chan and J. D. Goddard, Chem. Phys. Lett. **173**, 139 (1990).

[29] S. E. Sobottka and M. B. Williams, IEEE Trans. Nucl. Sci. **35**, 348 (1988).

[30] O. Jagutzki, V. Mergel, K. Ullmann-Pfleger, L. Spielberger, U. Meyer, R. Döner, and H. Schmidt-Böcking, "Fast position and time-resolved readout of microchannel plates with the delay-line technique for single particle and photon detection," in Proceedings in Imaging Spectroscopy IV, 322 San Diego, California, 1998.

[31] M. Lampton, O. Siegmund, and R. Raffanti, Rev. Sci. Instrum. **58**, 2298 (1987).

[32] J. Danielak, U. Domin, R. Kepa, M. Rytel, and M. Zachwieja, J. Mol. Spectrosc. **181**, 394 (1997).

[33] R. H. Judge and D. C. Moule, J. Mol. Spectrosc. **80**, 363 (1980).

[34] D. A. Prinslow and P. B. Armentrout, J. Chem. Phys. **94**, 3563 (1991).

[35] R. M. Joshi and J. Macromol. Sci., Chem. **A13**, 1015 (1979).

[36] J. Li and R. P. Steer, Can. J. Chem. **73**, 131 (1995).

[37] P. M. Regan, S. R. Langfold, D. Ascenzi, P. A. Cook, A. J. Orr-Ewing, and M. N. R. Ashfold, Phys. Chem. Chem. Phys. **1**, 3247 (1999).

[38] H. Okabe, J. Chem. Phys. **53**, 3507 (1970); *Photochemistry of Small Molecules* (Wiley–Interscience, New York, 1978).

[39] R. Schinke, *Photodissociation Dynamics, Cambridge Monographs on Atoms, Molecular and Chemical Physics 1* (Cambridge University Press, Cambridge, 1993).

[40] X. Chen, R. Marom, S. Rosenwaks, I. Bar, T. Einfeld, C. Maul, and K.-H. Gericke, J. Chem. Phys. **114**, 9033 (2001).

[41] T. Einfeld, C. Maul, K.-H. Gericke, R. Marom, S. Rosenwaks, and I. Bar, J. Chem. Phys. **115**, 6418 (2001).